EGU General Assembly 2020

tputs

Me.I.Ge.Pe.G

Metamorphic and Igneous Geo-Petrology Group

Università di Catania

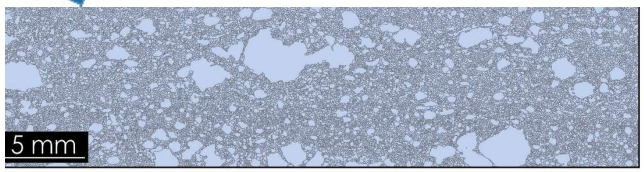

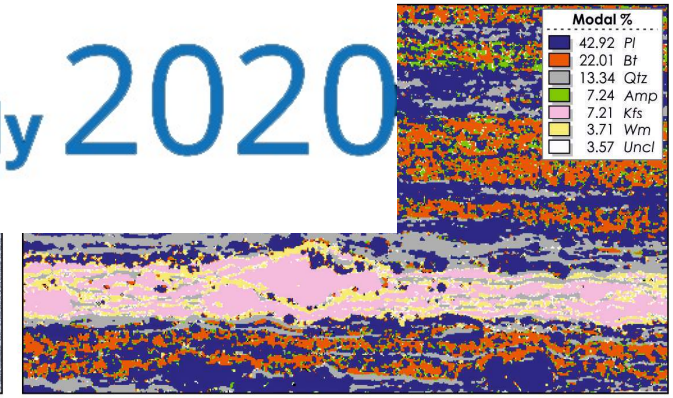

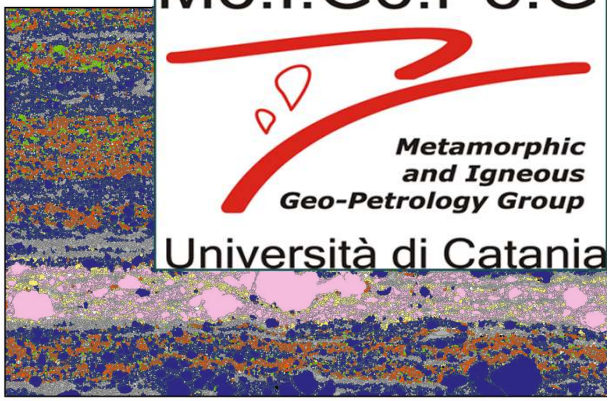

egend: Grain polygons (N_{Grains} = 102,710)

Legend: Amp Bt Kfs Pl Qtz Uncl Wm

Legend: N_{Amp}= 6,281 N_{Bt}= 19,820 N_{Kfs}= N_{Pl}= 32,628 N_{Qtz}= 11,461 N_{Wm}=

Quantitative microstructural analysis of western Mediterranean strike-slip kinematics: the Palmi Shear Zone, southern Calabria, Italy

Ortolano G.*1, Fazio E.1, Visalli R.1, Alsop I.2, Pagano M.1 & Cirrincione R.1

1-Dipartimento di Scienze Biologiche, Geologiche e Ambientali (DBGA), Università di Catania

2-*School of Geosciences - University of Aberdeen*

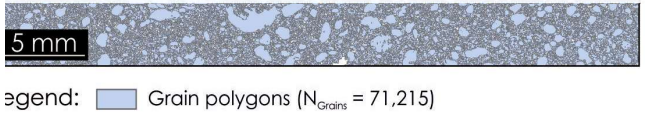

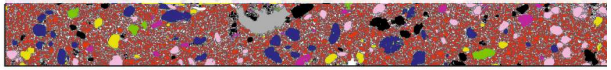

egend: Grain polygons (N_{Grains} = 71,215)

Legend: Amp Cc Cpx Kfs Pl Qtz Scap Talc Uncl Ca-min Fe-min K-min

Legend: N_{Amp}= 61 N_{Cc}= 26,097 N_{Cpx}= 2,612 N_{Kfs}= 1,582 N_{Pl}= N_{Scap}= 3,728 N_{Qtz}= 11 N_{Talc}= 600 N_{Ca-min}= 7,924 N_{Fe-min}= 547 N_{K-min}=

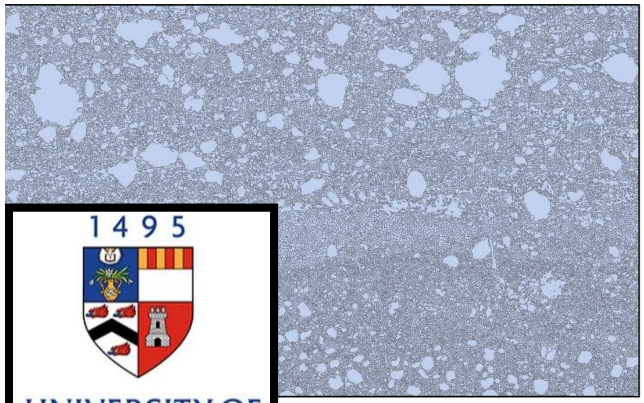

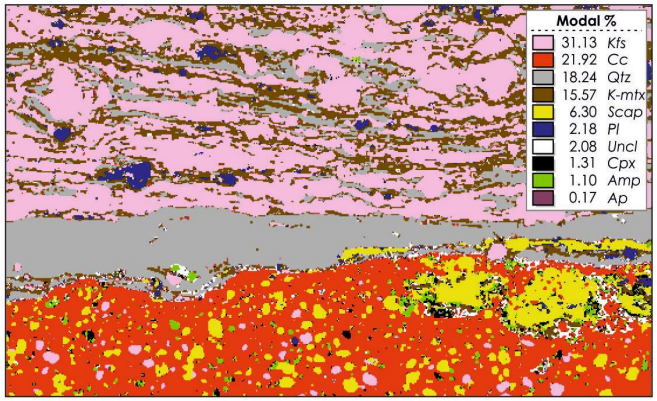

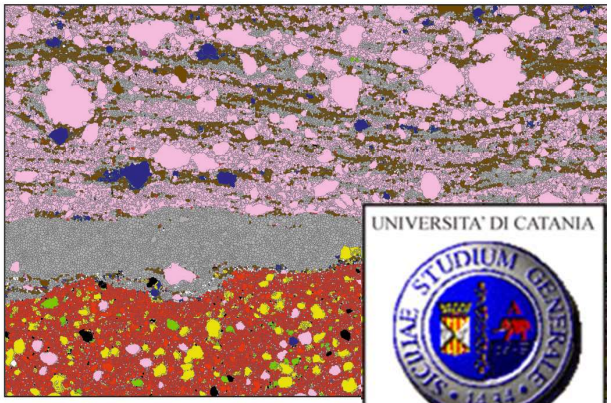

ns (N_{Grains} = 78,456)

Legend: Amp Ap Cc Cpx Kfs K-mtx Pl Qtz Scap Uncl

Legend: N_{Amp}= 857 N_{Ap}= 102 N_{Cc}= N_{K-mtx}= 10,259 N_{Pl}= 865 N_{Qtz}=

1495 UNIVERSITY OF ABERDEEN

UNIVERSITA' DI CATANIA STUDIUM GENERALE 1434 DIPARTIMENTO DI SCIENZE GEOLOGICHE

Quantitative image analysis of thin sections or polished slabs of deformed rocks is an essential step for extrapolating statistically meaningful fabric parameters

Many authors from the half of ’90 developed several methods to solve two main problems:

1) Grain Boundary Detections
2) Mineral phase recognition

Using several theoretical approaches and several kind of input images

Starting from the most used theoretical approaches, Supervised classification of μXRF maps were here combined with elaboration derived from high-resolution thin section scans within new GIS-based package tools, specified for structural analysis

HD thin section scans

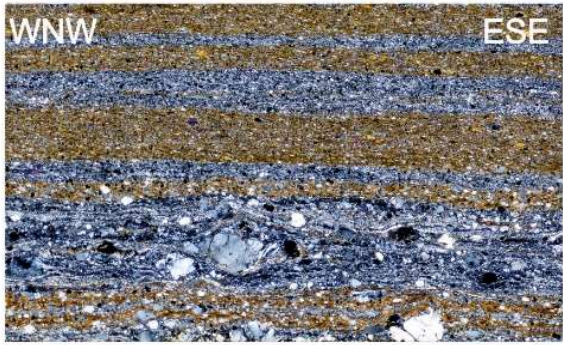

Classified thin section image

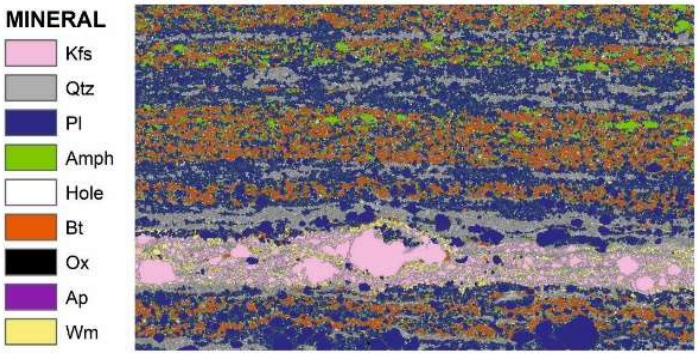

Fabric analysis of porphyroclast

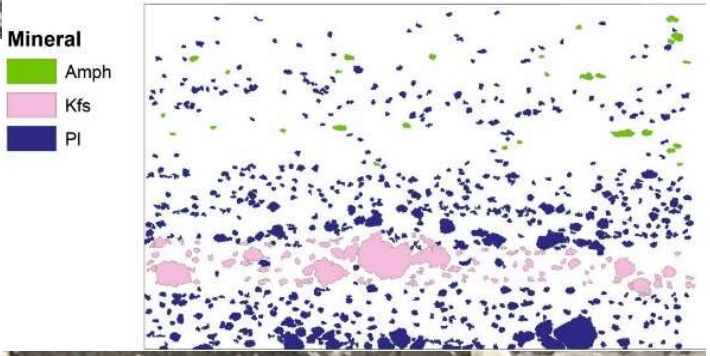

Most of the used algorithms for segmentation and grain boundaries detection purposes are implemented in many image processing software

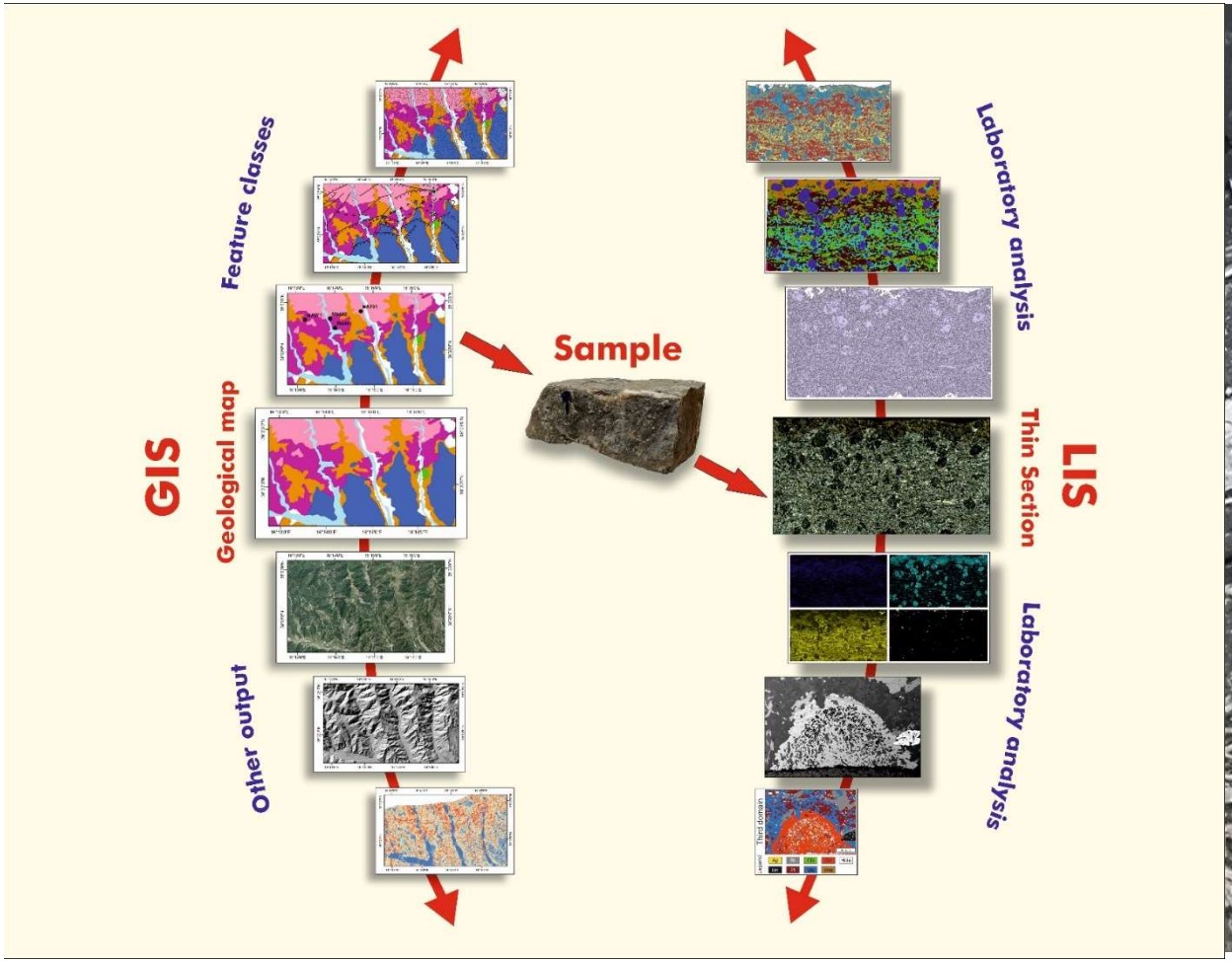

ArcGIS

python

Nevertheless just few of them well integrate most of the best performed ones with the possibility to automatize them in complex operational sequences, storing at the same time all the potential derivative mineral-chemical and textural features within a user-friendly database

These new tools allows the users to quantitatively extrapolate several microstructural features such as **grain size and grain shape distribution of all of the grains subdivided per mineral types**

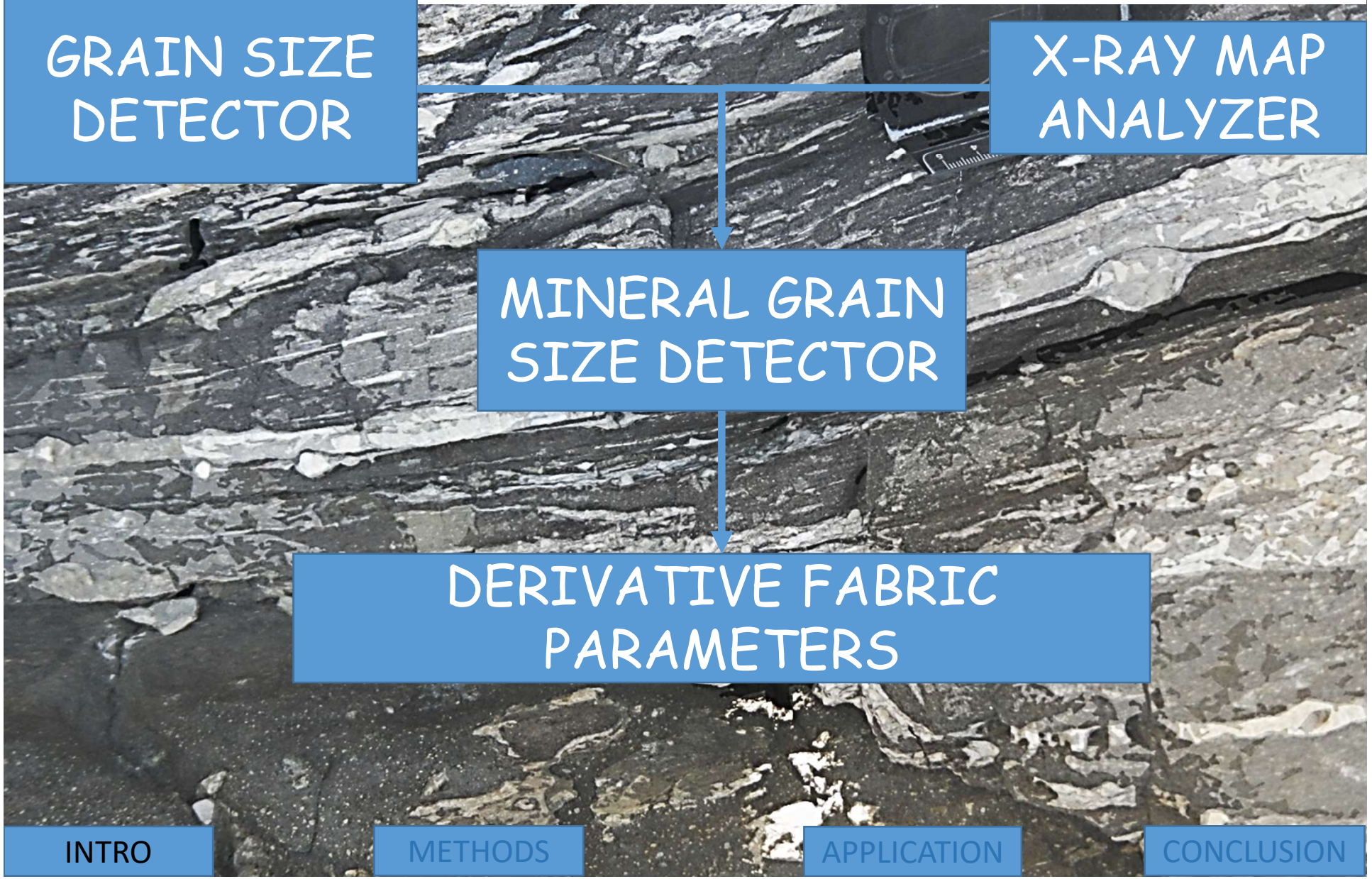

Grain Size Detector (GSD):
Input image and graphical interface

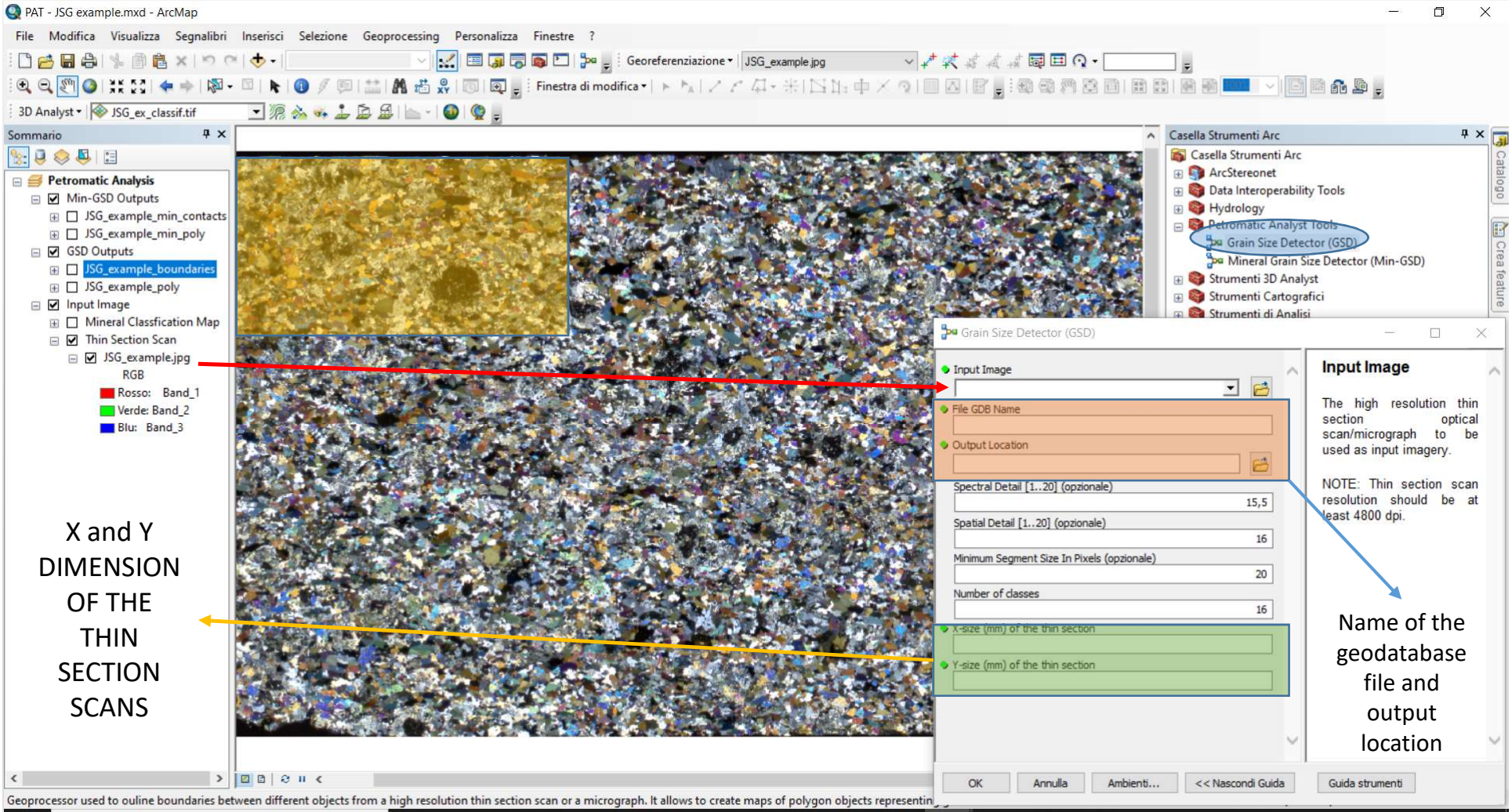

Grain Size Detector (GSD):
Output of the Grain Size Detection

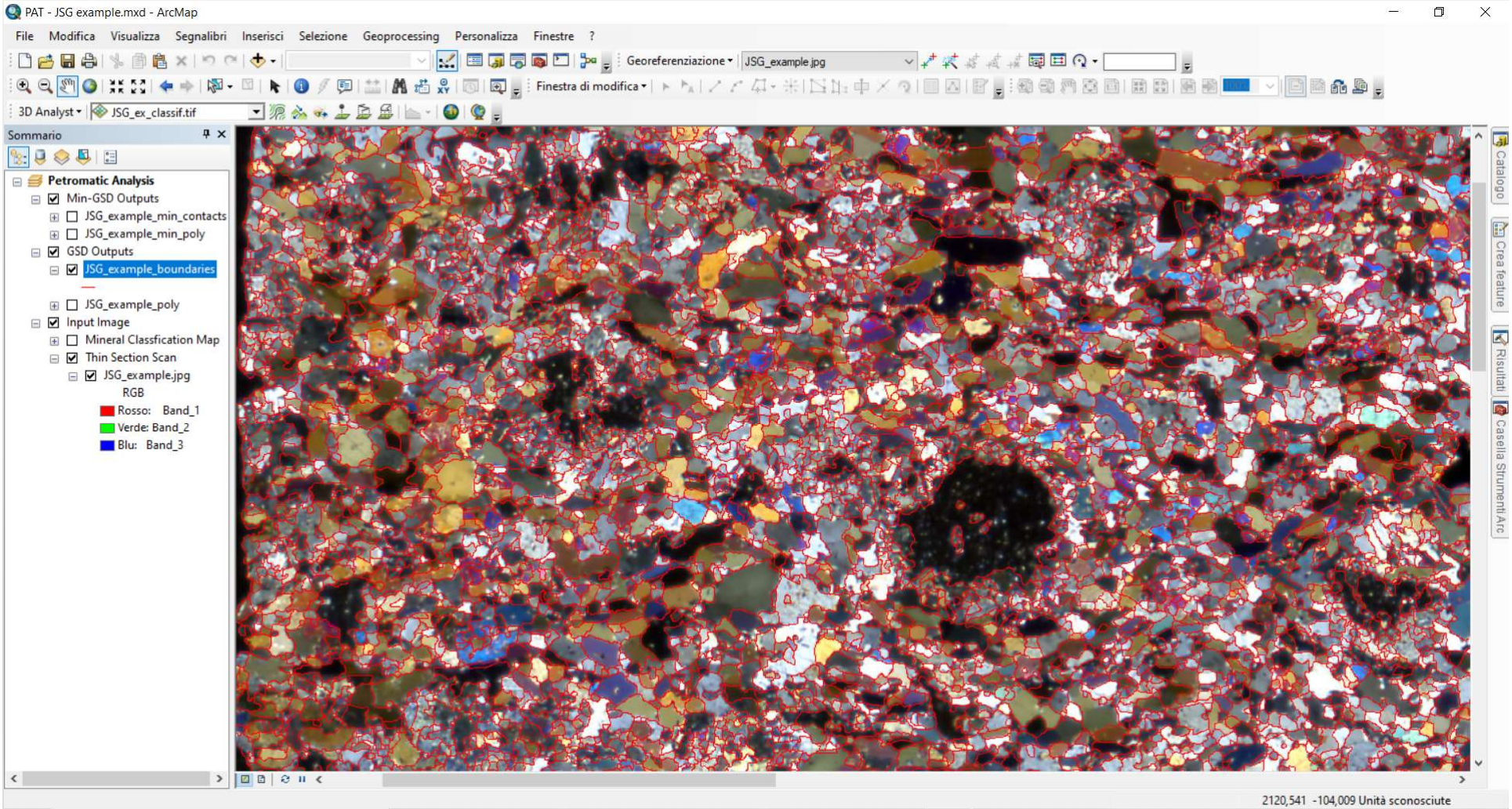

Grain Size Detector (GSD): Output of the Minimum Boundary Geometry algorithm

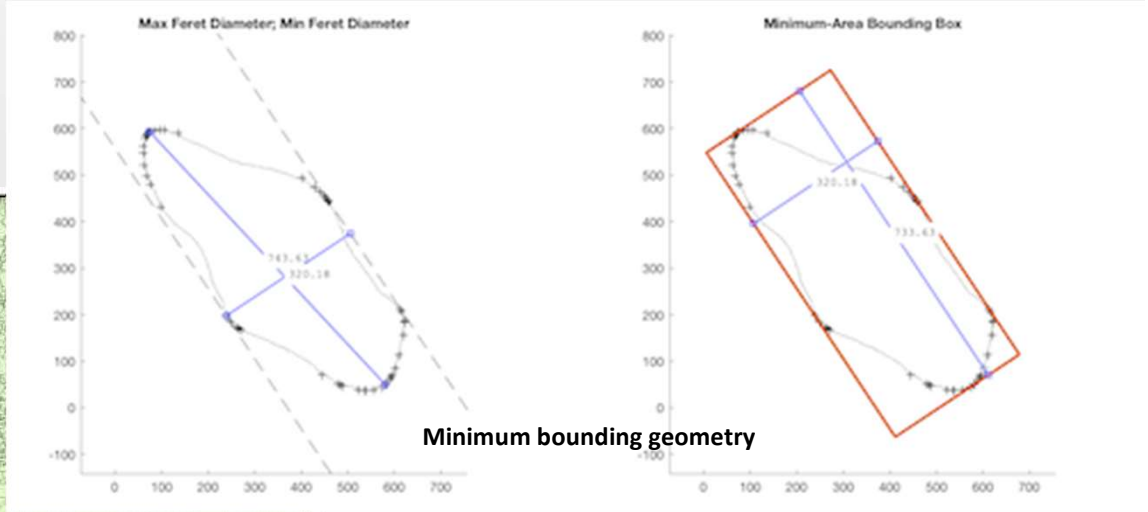

Minimum bounding geometry

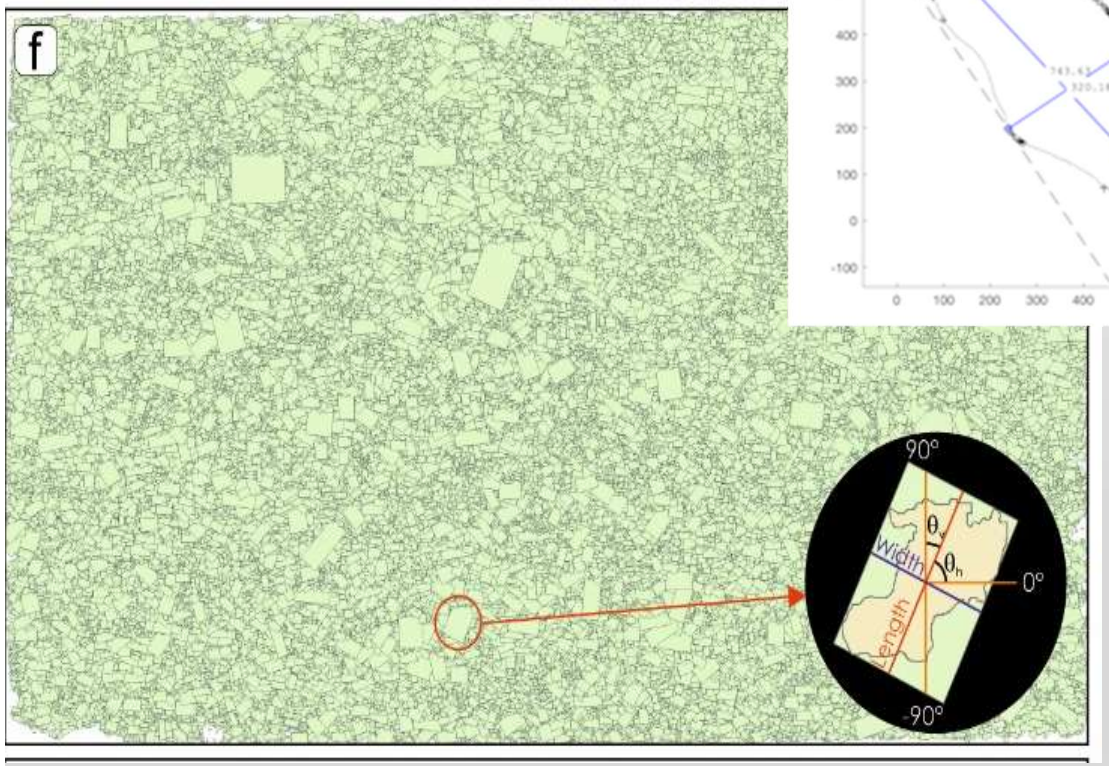

Mineral Grain Size Descriptors

Fundamental Size factors

Grain Area (A)
(Total number of pixel within polygon)

Grain Perimeter (P)
(Total number of pixel along grain boundary)

Grain Length (L)
(Total number of pixel along the long axis)

Grain Width (W)
(Total number of pixel along the short axis)

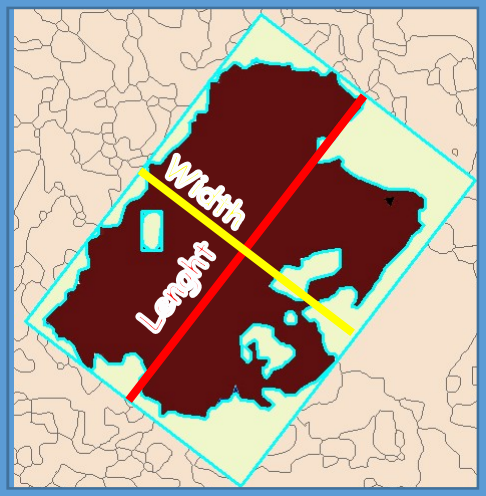

Conversion factors

(Xmm / Xpx) * (Ymm / Ypx) * Grain Area

(((Xmm / Xpx) + (Ymm / Ypx)) / 2) * Grain Perimeter

(((Xmm / Xpx) + (Ymm / Ypx)) / 2) * Grain Length

(((Xmm / Xpx) + (Ymm / Ypx))) / 2) * Grain Width

Mineral-Grain Shape Factors

Derivative shape factors

Grain Orientation

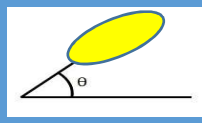

Elongation (E)

$E = (\pi * L^2) / (4*A)$

Compactness (Cp)

$$Cp = \frac{P^2}{4\pi A}$$

EQPC Diameter

$$D_a = 2\sqrt{\frac{A}{\pi}}$$

Roundness (R)

$$R = \frac{4A}{\pi L^2} = 1/E$$

Straightness (S)

$S = L / P$

Axial Ratio (AR)

$$AR = \frac{L}{W}$$

Circularity (C)

$$C = \frac{4A}{PL}$$

Grain Shape Factor (GSF)

Grain shape factor $$GSF = \left(L/W\right)^{0.318} \cdot \frac{P}{2\sqrt{A}}$$

Aspect Ratio (AsR) and Bretherton shape factor

$$AsR = \frac{1}{AR} = \frac{W}{L}$$

$$B^* = \left(M_x^2 - M_n^2\right) / \left(M_x^2 + M_n^2\right)$$

Ellipticity (El)

$$El = \frac{\pi L^2}{2A}$$

Grain Shape Index (GSI)

Grain shape index $$GSI = \frac{2\pi\sqrt{A/\pi}}{L}$$

Grain Size Detector (GSD):
Plot of the grains clustered per roundness index

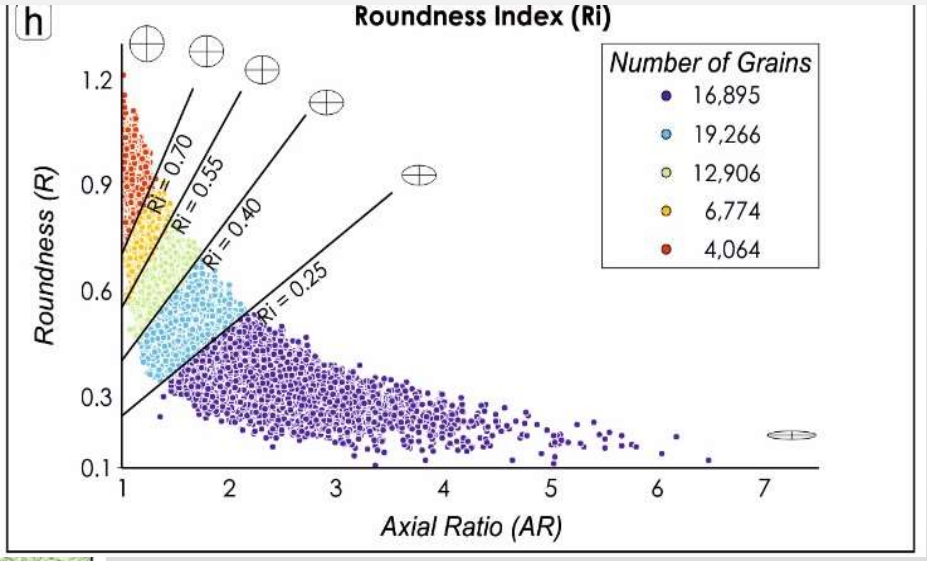

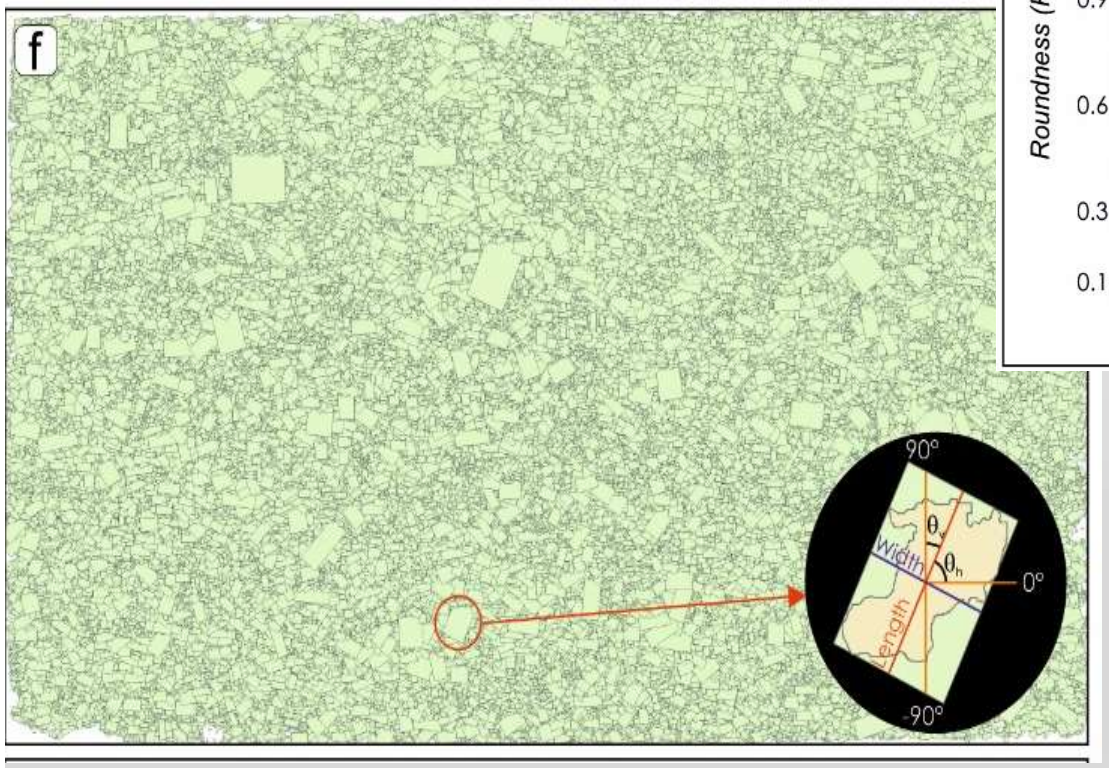

XRMA vs. Q-XRMA

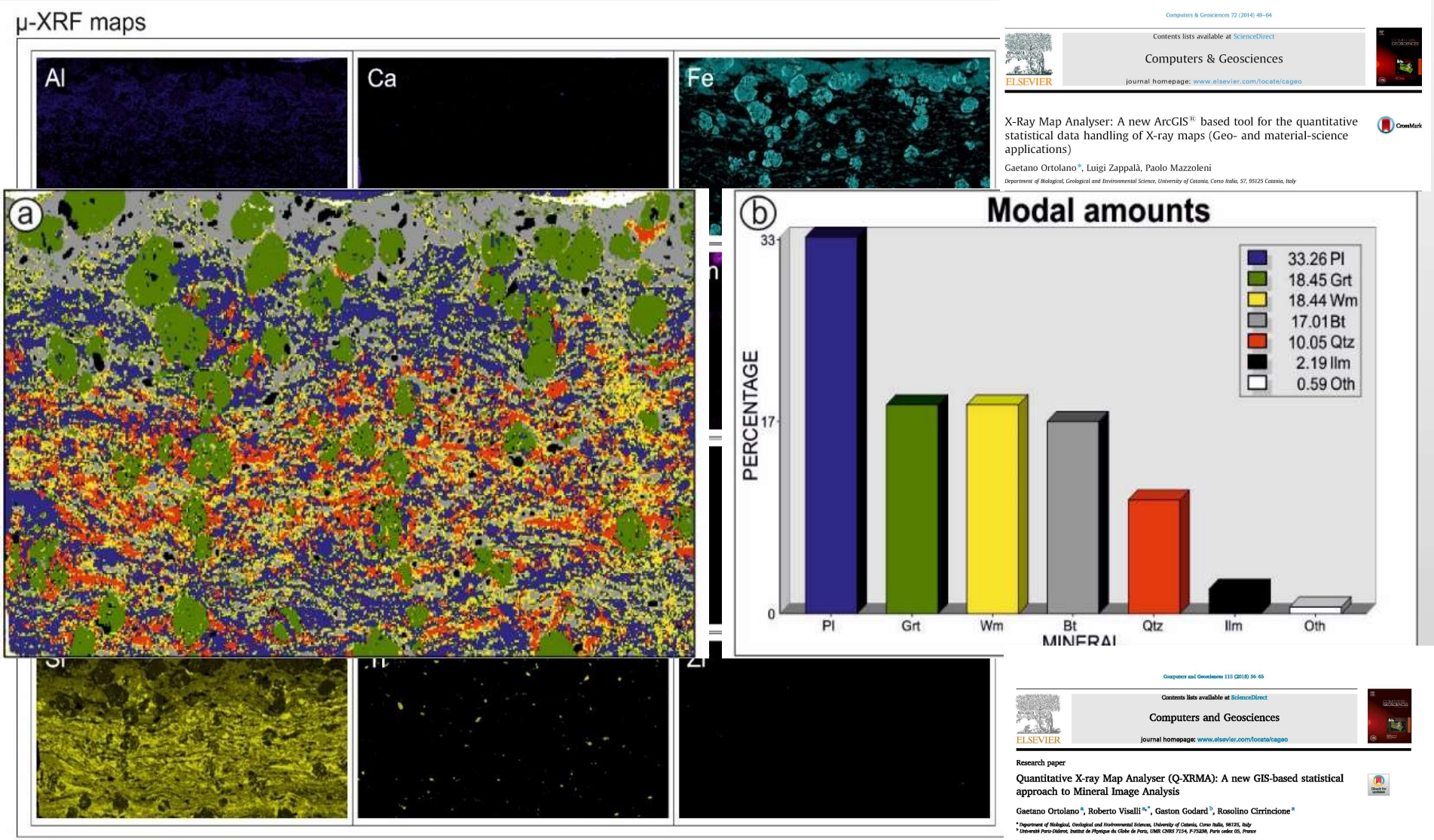

Computers & Geosciences 72 (2014) 49–64

Contents lists available at ScienceDirect

Computers & Geosciences

journal homepage: www.elsevier.com/locate/cageo

X-Ray Map Analyser: A new ArcGIS® based tool for the quantitative statistical data handling of X-ray maps (Geo- and material-science applications)

Gaetano Ortolano*, Luigi Zappalà, Paolo Mazzoleni

Department of Biological, Geological and Environmental Science, University of Catania, Corso Italia, 57, 95125 Catania, Italy

Computers and Geosciences 115 (2018) 56–65

Contents lists available at ScienceDirect

Computers and Geosciences

journal homepage: www.elsevier.com/locate/cageo

Research paper

Quantitative X-ray Map Analyser (Q-XRMA): A new GIS-based statistical approach to Mineral Image Analysis

Gaetano Ortolano[a], Roberto Visalli[a,*], Gaston Godard[b], Rosolino Cirrincione[a]

[a] Department of Biological, Geological and Environmental Sciences, University of Catania, Corso Italia, 95125, Italy

[b] Université Paris-Diderot, Institut de Physique du Globe de Paris, UMR CNRS 7154, F-75238, Paris cedex 05, France

Mineral Grain Size Detection - MinGSD

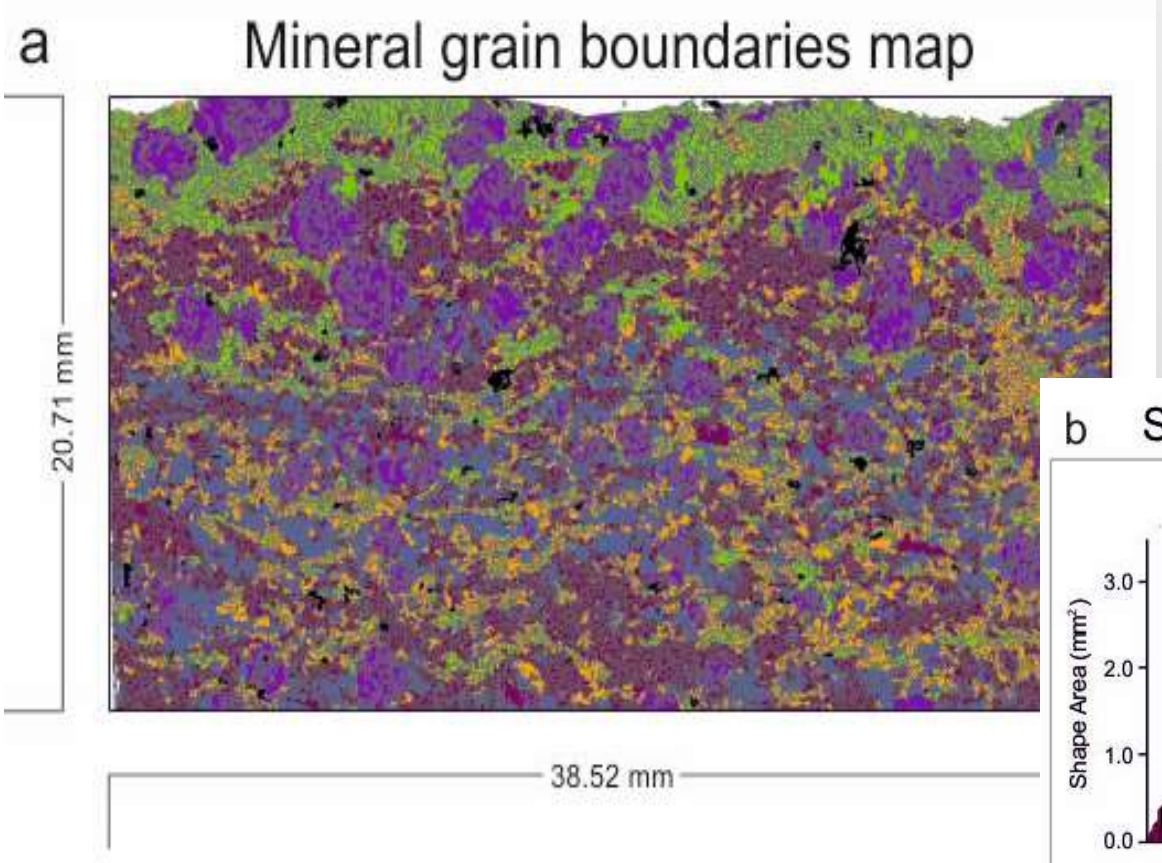

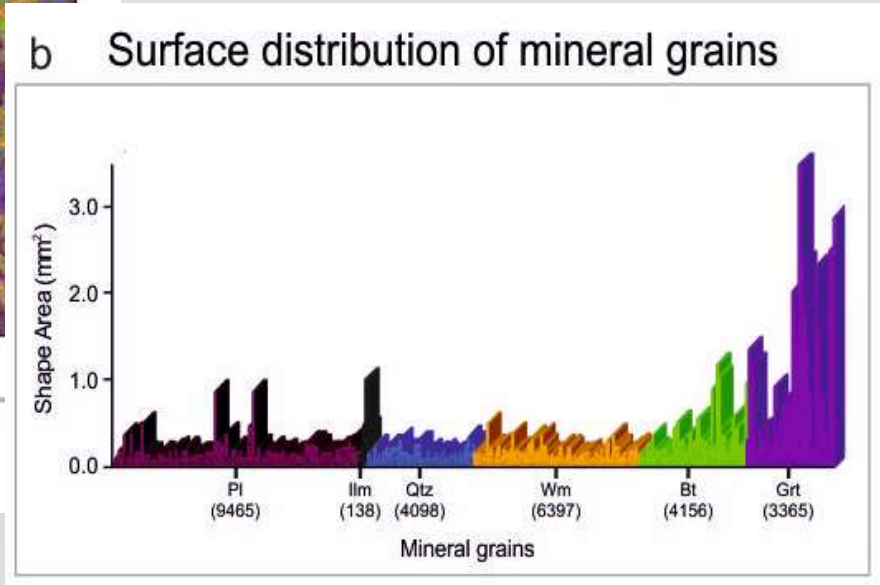

Mineral Grain Size Detection - MinGSD

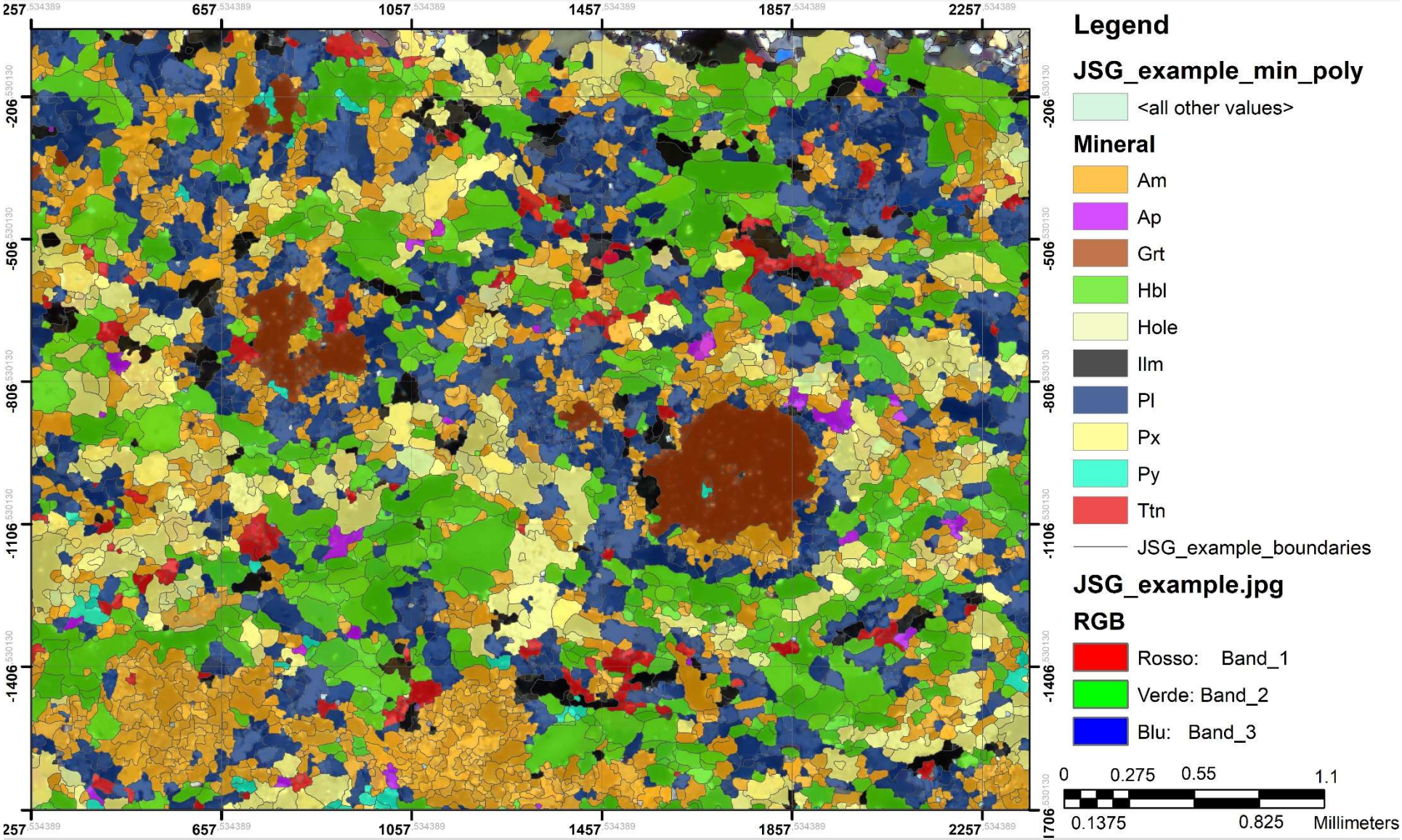

EXAMPLE OF ALPHANUMERICAL DERIVATIVE DATA AUTOMATICALLY CALCULATED FOR EACH RECOGNISED GRAIN

OBJECTID	1	2	3	4	5	6	…..n
Long Axis (mm)	0,429	0,587	0,806	1,291	0,373	0,336	0,450
Short Axis (mm)	0,233	0,349	0,318	0,376	0,306	0,280	0,404
Angle of Long axis perpendicular to the main foliation	90,000	90,000	74,358	90,000	159,775	70,560	70,346
Axial Ratio (R)	1,841	1,682	2,536	3,437	1,218	1,200	1,116
Aspect Ratio	0,543	0,595	0,394	0,291	0,821	0,833	0,896
Area (mm2)	0,072	0,158	0,182	0,333	0,087	0,063	0,129
Elongation	2,008	1,712	2,795	3,928	1,254	1,413	1,231
Roundness	0,498	0,584	0,358	0,255	0,797	0,708	0,813
Perimeter	1,193	1,744	1,989	3,331	1,211	1,122	1,537
Circularity	0,562	0,618	0,455	0,310	0,771	0,666	0,747
Compactness	1,578	1,531	1,727	2,653	1,340	1,595	1,455
Grain Shape Index	2,216	2,400	1,878	1,584	2,804	2,642	2,830
Grain Shape Factor	2,702	2,586	3,131	4,274	2,185	2,371	2,213
Straightness	0,359	0,337	0,405	0,387	0,308	0,300	0,293
Equal Area Projected Circle Diameter (mm)	0,302	0,449	0,482	0,651	0,333	0,283	0,406
Ellipticity	4,017	3,424	5,589	7,856	2,508	2,826	2,461
Angle of Long axis with respect the main foliation	0,000	0,000	15,642	0,000	-69,775	19,440	19,654
Mineral	Pl	Pl	Pl	Pl	Pl	Pl	Pl
B* (Bretherton shape factor))	0,544	0,478	0,731	0,844	0,195	0,180	0,109

CASE STUDY: THE ROLE OF THE ALPINE STRIKE SLIP TECTONICS IN THE WESTERN MEDITERRANEAN GEODYNAMICS

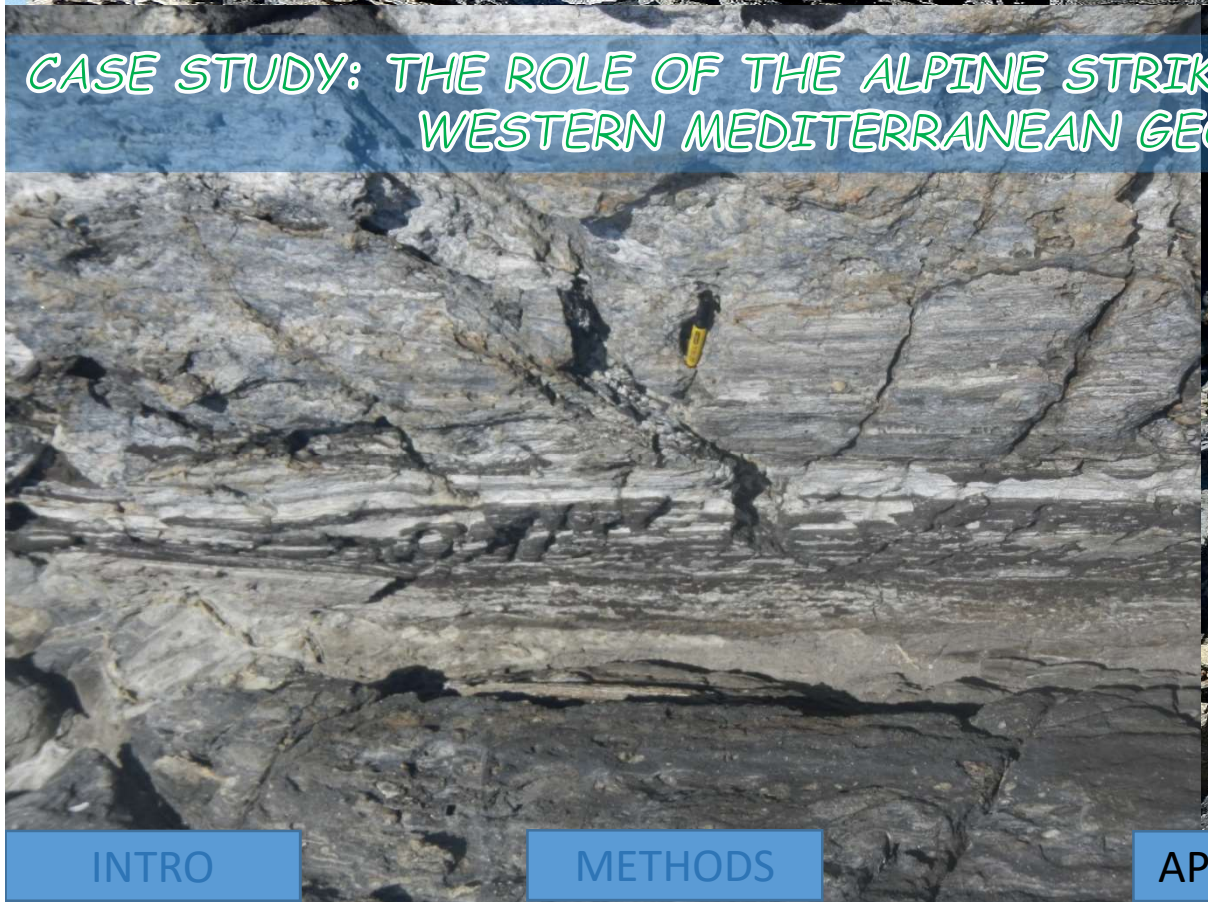

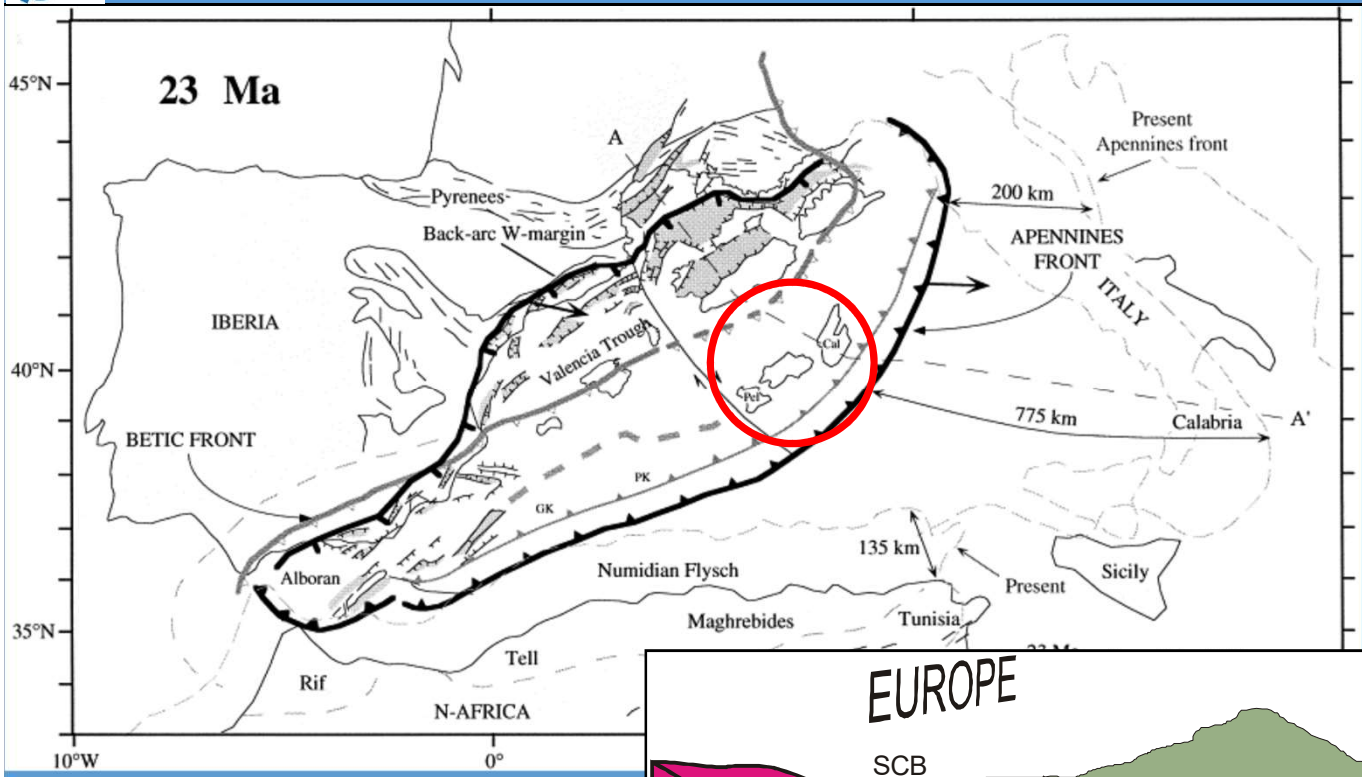

Reconstruction of the tectonic evolution of the western Mediterranean since the Oligocene - Rosenbaum, G., Lister, G. and Duboz, C. 2002.

Cirrincione, R., Fazio, E., Fiannacca, P., Ortolano, G., Pezzino, A., Punturo, R. (2015) Periodico di Mineralogia, 84 (3B)

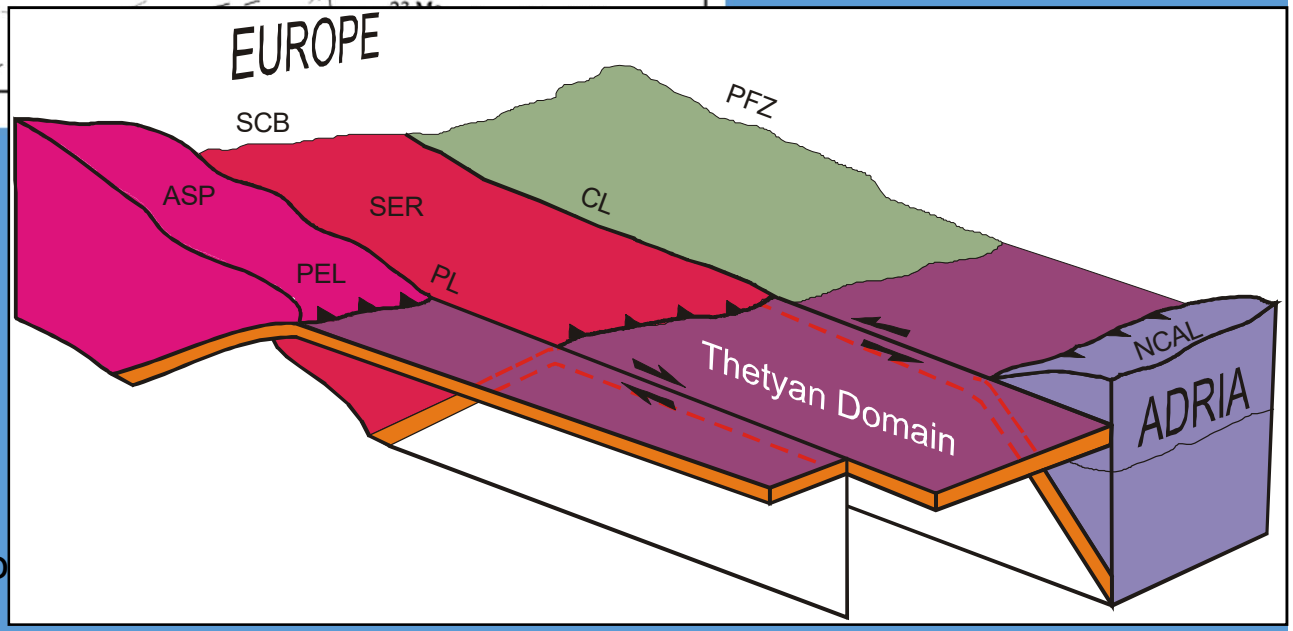

3D Block diagram of the pre-collisional paleo-geodynamic scenario of the CPO within the central Mediterranean area (NCAL: Northern Calabria; ASP: Aspromonte; PEL: Peloritani; SER: Serre; SCB: Sardinia Corsica Block; PL: Palmi Line; CL: Catanzaro Line; PFZ: Pollino Fault Zone).

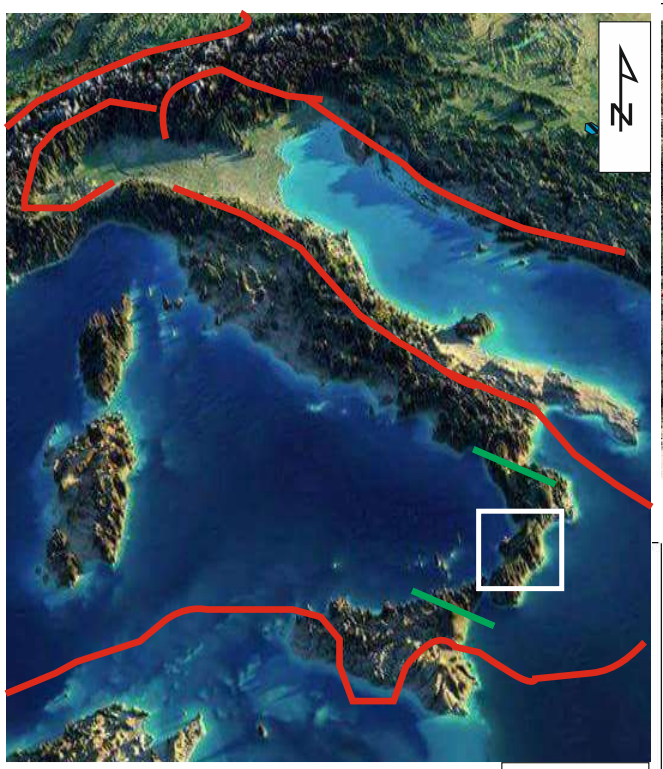

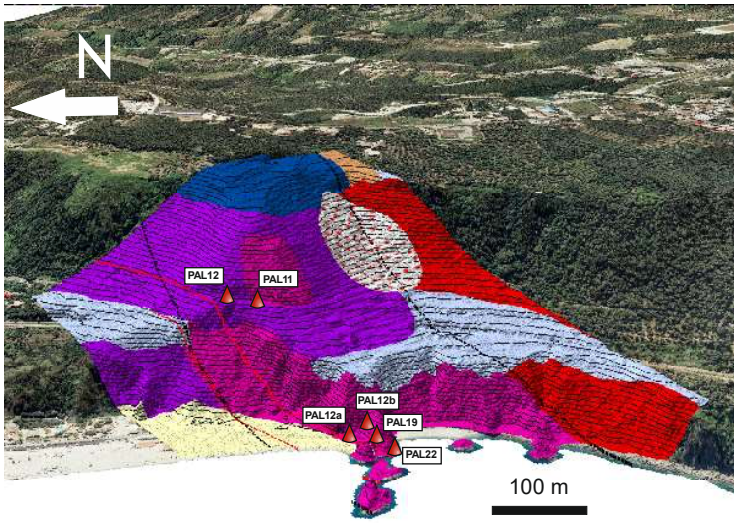

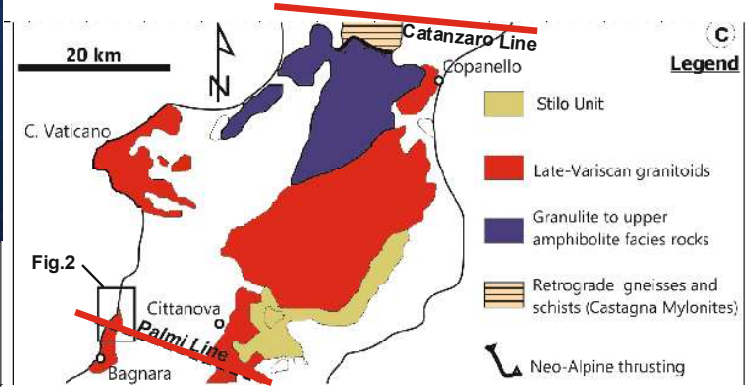

Legend

Lithotypes

- Siliciclastic arenites
- Marly clays
- Porites limestones
- Clastic limestones
- Debris (?)
- Landslides
- Gneiss occhiadini
- Tonalites
- Migmatitic paragneiss
- Skarns
- Alluvial deposits
- Marine terraces
- Trubi

Symbols

- Shear zone boundaries
- Normal fault (certain)
- Normal fault (presumed)
- Samples

MICR PLES

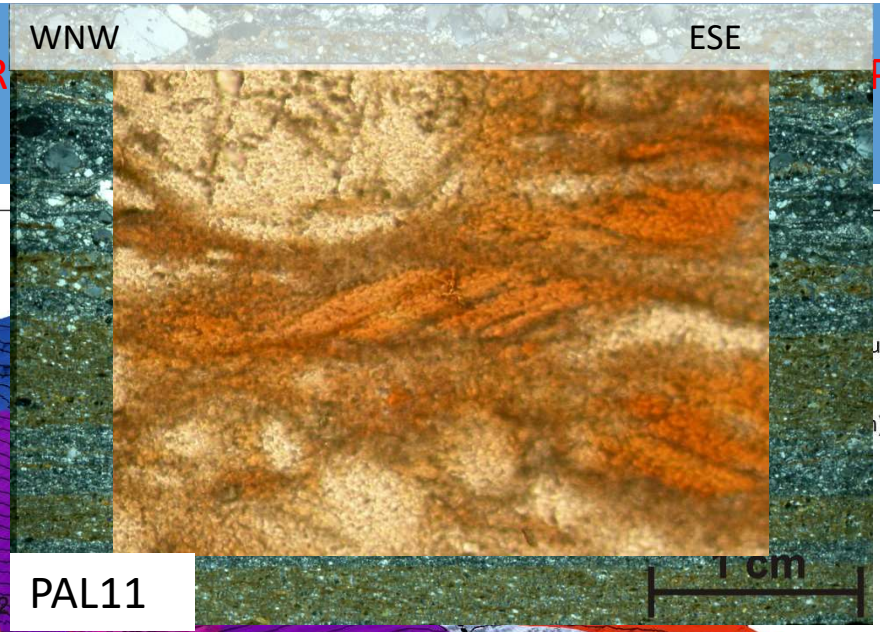

PAL11

PAL12A

PAL 22

INPUT IMAGES

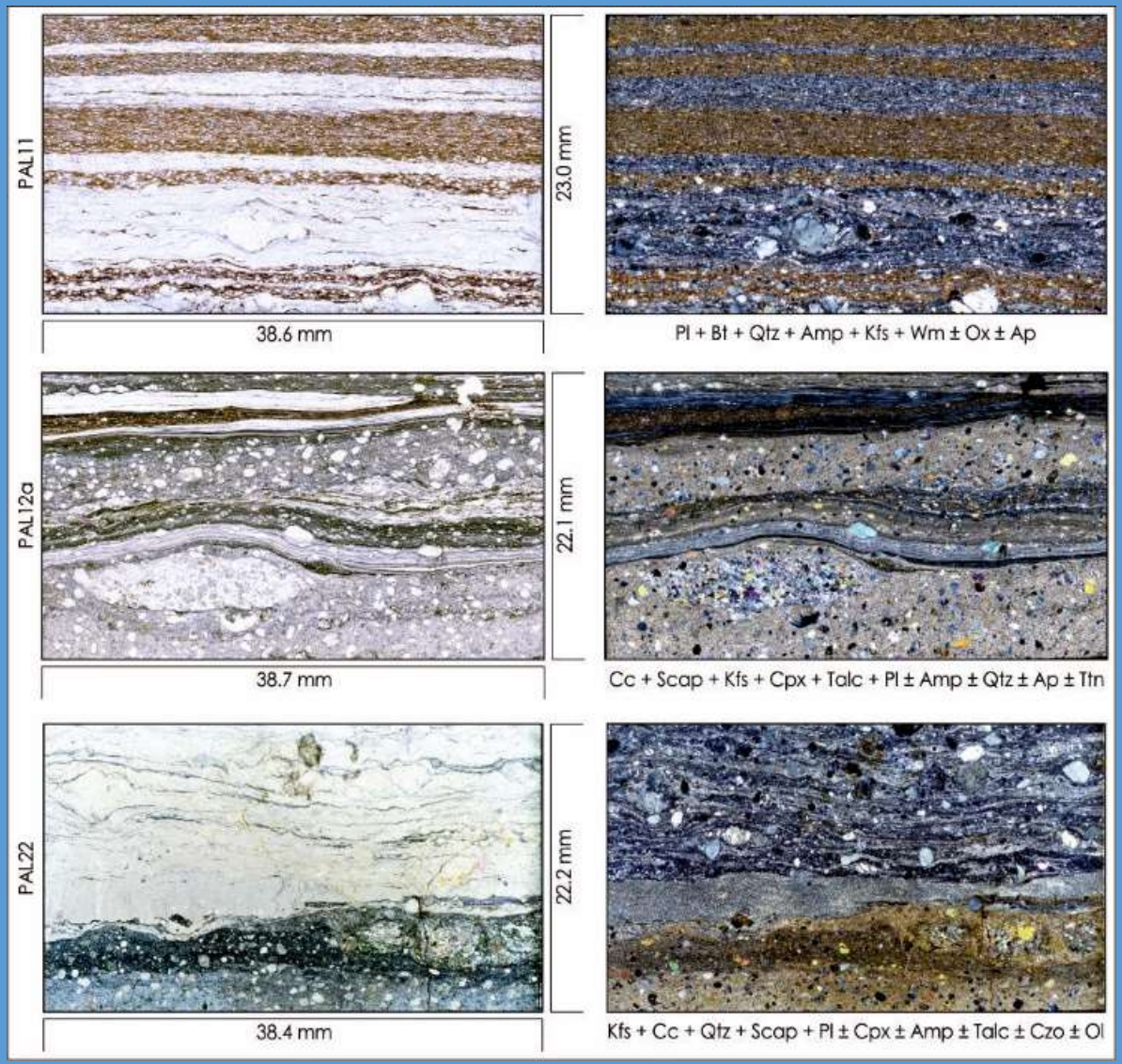

RESULTS

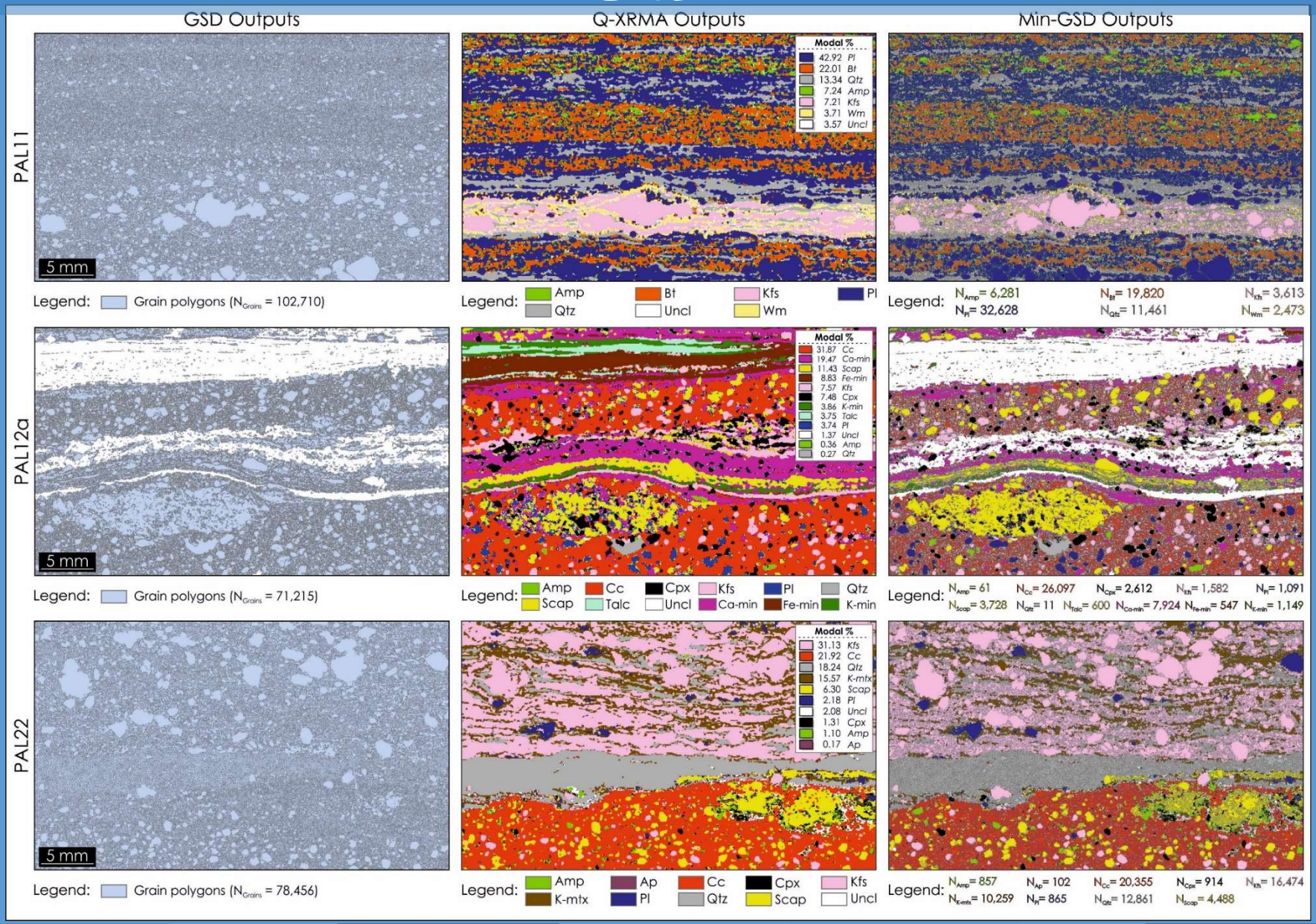
GSD Outputs
Q-XRMA Outputs
Min-GSD Outputs
PAL11
PAL12a
PAL22
5 mm
Legend: Grain polygons (N_Grains = 102,710)
Legend: Grain polygons (N_Grains = 71,215)
Legend: Grain polygons (N_Grains = 78,456)
Modal %
42.92 Pl
22.01 Bt
13.34 Qtz
7.24 Amp
7.21 Kfs
3.71 Wm
3.57 Uncl
Legend: Amp Bt Kfs Pl Qtz Uncl Wm
N_Amp= 6,281 N_Bt= 19,820 N_Kfs= 3,613 N_Pl= 32,628 N_Qtz= 11,461 N_Wm= 2,473
Modal %
31.87 Cc
19.47 Ca-min
11.43 Scap
8.83 Fe-min
7.57 Kfs
7.48 Cpx
3.86 K-min
3.75 Talc
3.74 Pl
1.37 Uncl
0.36 Amp
0.27 Qtz
Legend: Amp Cc Cpx Kfs Pl Qtz Scap Talc Uncl Ca-min Fe-min K-min
N_Amp= 61 N_Cc= 26,097 N_Cpx= 2,612 N_Kfs= 1,582 N_Pl= 1,091 N_Scap= 3,728 N_Qtz= 11 N_Talc= 600 N_Ca-min= 7,924 N_Fe-min= 547 N_K-min= 1,149
Modal %
31.13 Kfs
21.92 Cc
18.24 Qtz
15.57 K-mtx
6.30 Scap
2.18 Pl
2.08 Uncl
1.31 Cpx
1.10 Amp
0.17 Ap
Legend: Amp Ap Cc Cpx Kfs K-mtx Pl Qtz Scap Uncl
N_Amp= 857 N_Ap= 102 N_Cc= 20,355 N_Cpx= 914 N_Kfs= 16,474 N_K-mtx= 10,259 N_Pl= 865 N_Qtz= 12,861 N_Scap= 4,488

DERIVATIVE DATA ELABORATION

Porphyroclast domains

PAL11

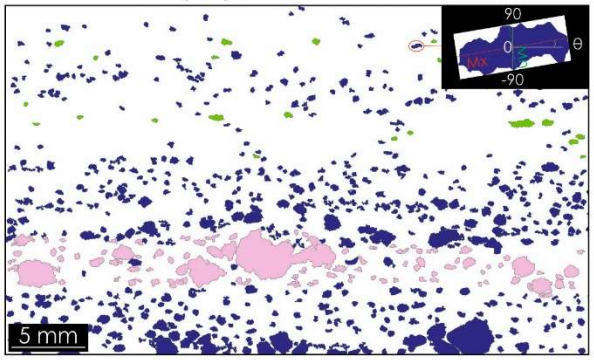

Legend: N_{Amp}= 30 N_{kfs}= 100 N_{Pl}= 604

PAL12a

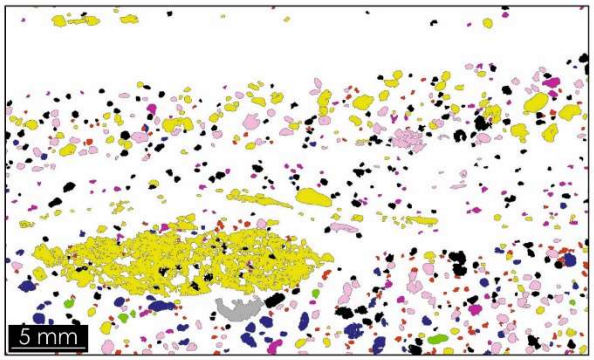

Legend: N_{Amp}= 6 N_{Pl}= 63 N_{Cc}= 144 N_{Qtz}= 1 N_{Cpx}= 231 N_{Scap}= 187 N_{Kfs}= 149 $N_{Co\text{-}min}$= 102

PAL22

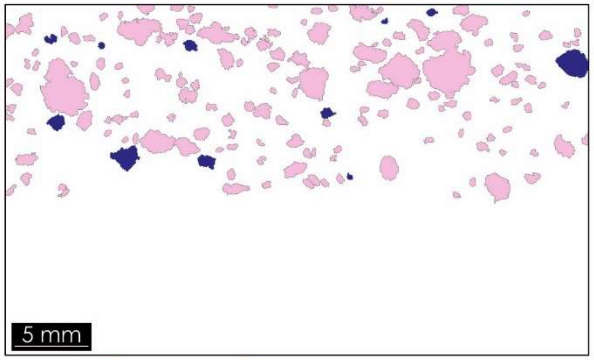

Legend: N_{Kfs}= 145 N_{Pl}= 11

R vs. θ graph

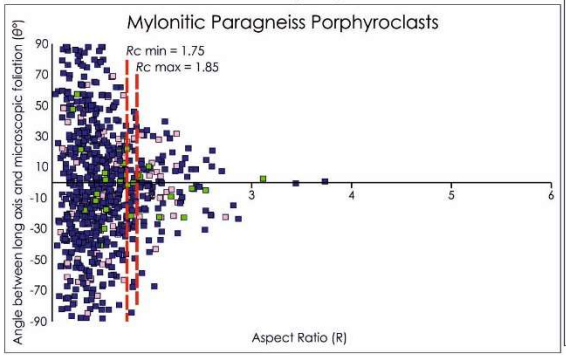

W_m = 0.51 - 0.55

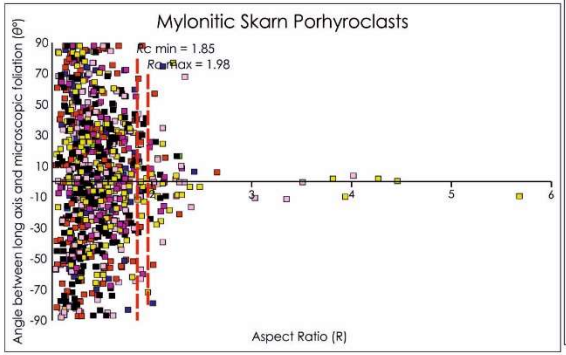

W_m = 0.55 - 0.59

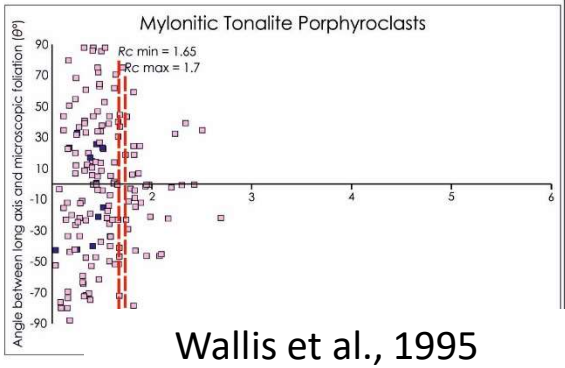

Wallis et al., 1995

Rigid Grain Net Analysis

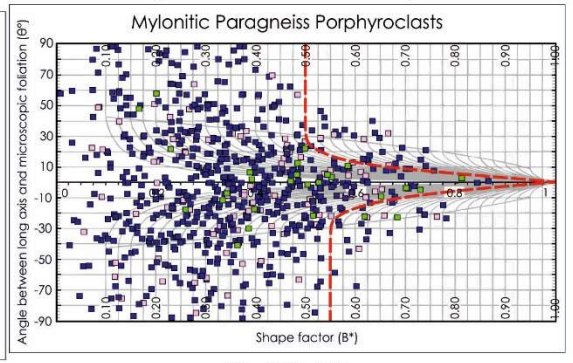

W_m = 0.50 - 0.55

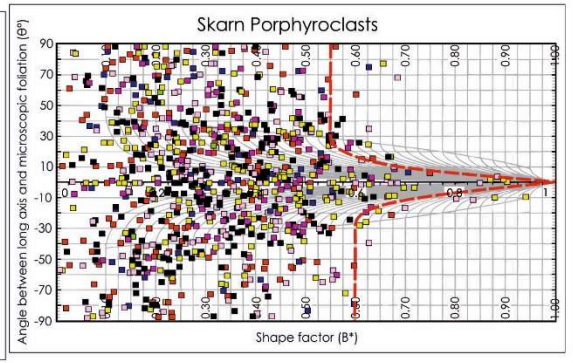

W_m = 0.55 - 0.60

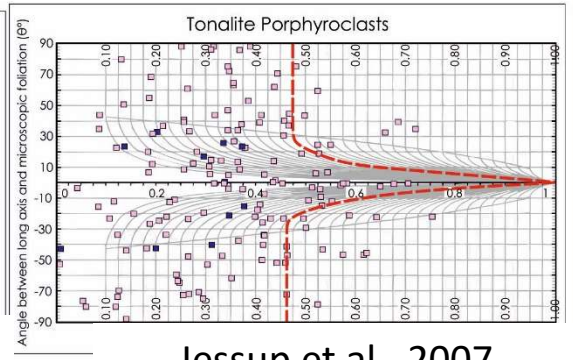

Jessup et al., 2007

RIGID GRAIN NET ANALYSIS:
SUB-SIMPLE SHEAR PERCENTAGE EXTRAPOLATION

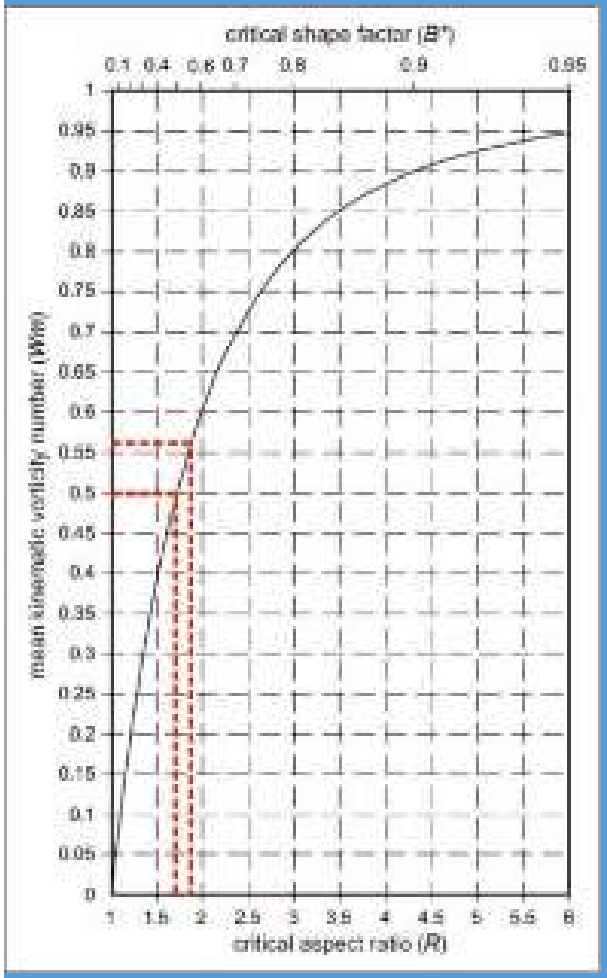

Wallis et al., 1995

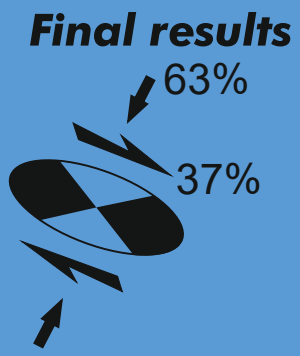

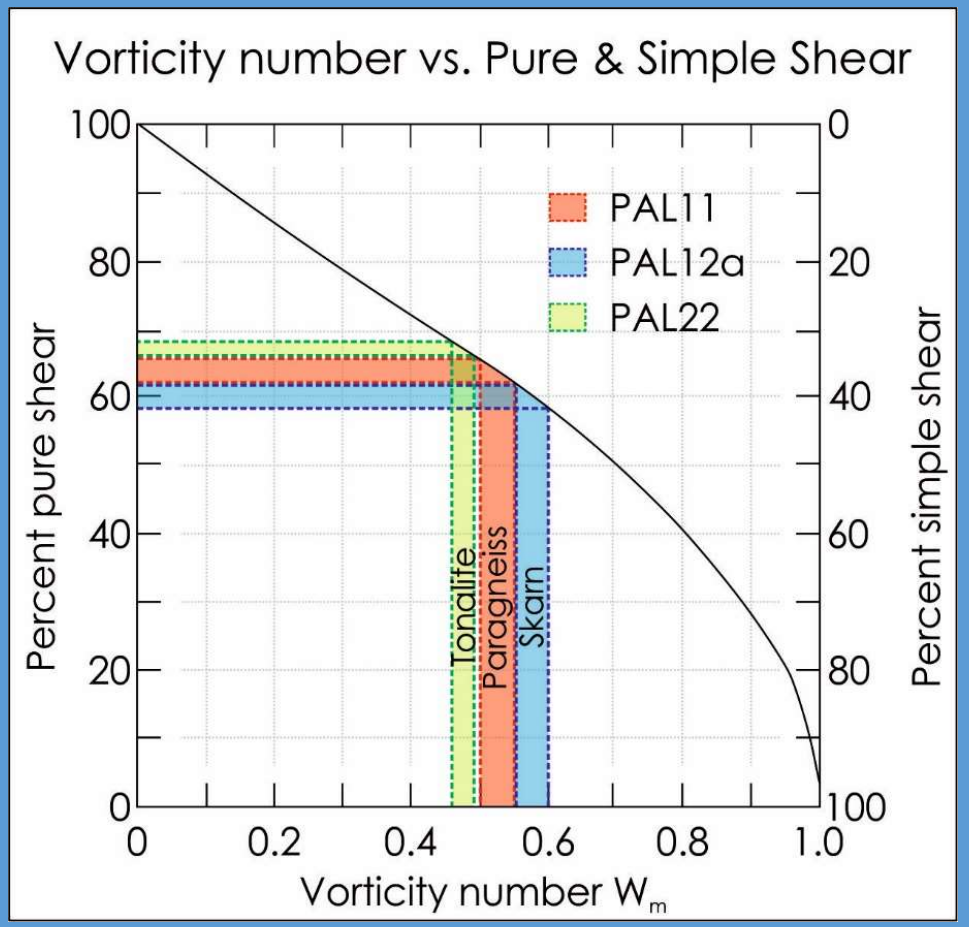

Law et al., 2004

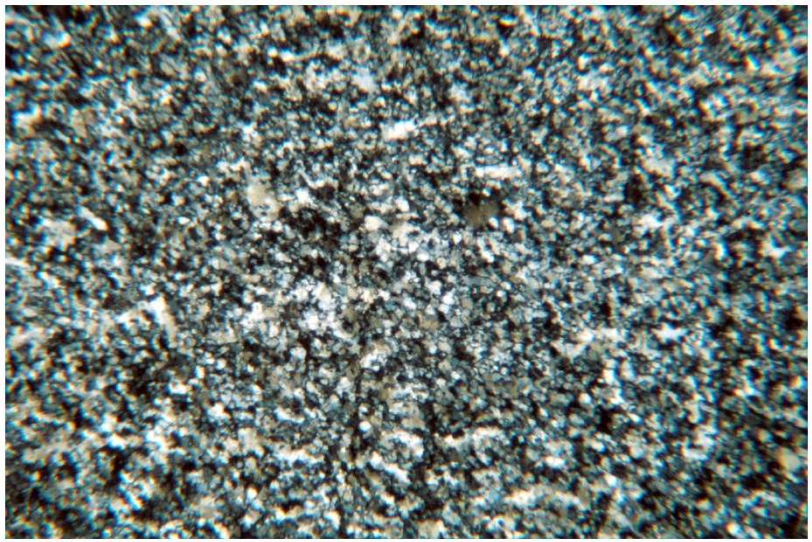

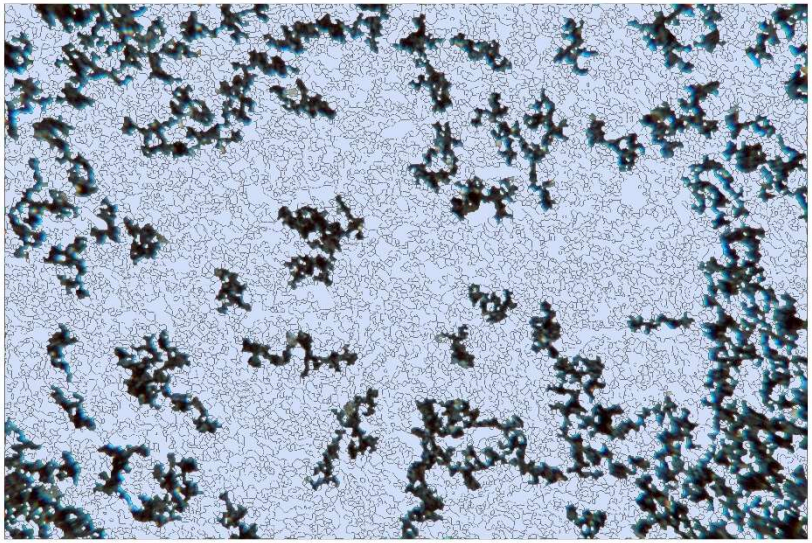

Syn-mylonitic quartz grain boundaries analysis

Recrystallization regime: SGR and GBM

Quartz average grain-size 18 μm

$$\dot{\varepsilon} = A\,\sigma^{n}\,f_{H_2O}^{m}\,e^{(-Q/RT)}$$

Schimizu (2008) paleopiezometer

Preliminary shear Strain Rate $\dot{\varepsilon}$° = 1,13E-11 1/s

The Micro-structural study of the PSZ allowed to affirm that:

1. Rock-types involved in the mylonitic shearing activity are characterized by a sub-vertical foliation mostly accommodated by the skarns and subordinately developed also in the tonalite and in the migmatitic paragneiss where the deformation tend to concentrate defining several narrow shear zones;
2. Image analysis of porphyroclastic domains has been used to infer the dominant shear-type through Rigid Grain Analysis, revealing a pure shear component of 66 to 68 % for the mylonitic tonalites; 62 to 66 % for the mylonitic paragneisses; and 58 to 62 % for the mylonitic skarn;
3. The shear strain rate, calculated on syn-mylonitic recrystallized quartz grains, ranges on average from 1.14*10-12 (1/s) for mylonitic paragneiss to 5.91*10-12 (1/s) for mylonitic tonalite, and is in accord with high strain zones in natural settings, applying the paleopiezometer of Shimizu (2008).

EGU General Assembly 2020

Me.I.Ge.Pe.G
Metamorphic and Igneous Geo-Petrology Group
Università di Catania

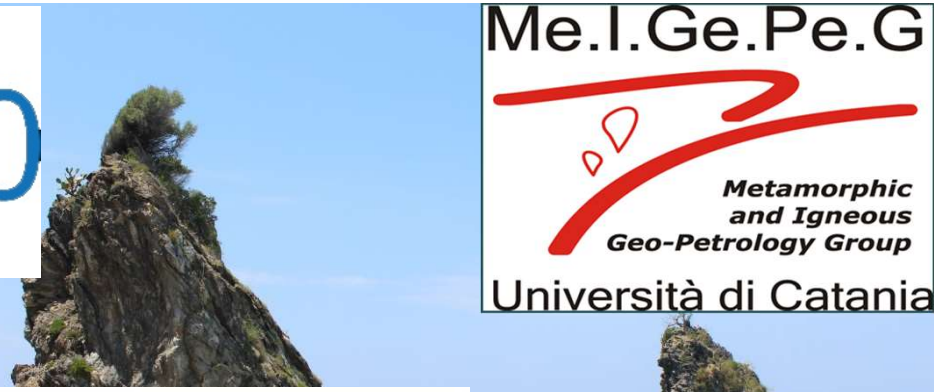

Thank you very much for your attention from our research group and see you for the next DRT in Catania

1495
UNIVERSITY OF ABERDEEN

UNIVERSITA' DI CATANIA
STUDIUM GENERALE
1434
DIPARTIMENTO DI SCIENZE GEOLOGICHE

Cited references

Ortolano, G., Fazio, E., Visalli, R., Alsop, G.I., Pagano, M., Cirrincione, R. 2020. Journal of Structural Geology, 131, art. no. 103956.

1. Cirrincione, R., Fazio, E., Fiannacca, P., Ortolano, G., Pezzino, A., Punturo, R. (2015). Period. Mineral., 84(3B), 701-749.
2. Fazio E., Ortolano G., Visalli A., Cirrincione R., Pezzino R., (2018). Ital. J. Geosci., Vol. 137 (2018). (https://doi.org/10.3301/IJG.2018.09).
3. Fazio, E., Ortolano, G., Cirrincione, R. (2017). International Journal of Earth Sciences, 106.
4. Jessup M.J., Law R.D. & Frassi C. (2007). J. Struct. Geol., 29(3), 411-421.
5. Ortolano G, Cirrincione R, Pezzino A, Puliatti, G (2013). Rend. online Soc. Geol. Ital., vol. 29.
6. Ortolano, G., Visalli, R., Godard, G., Cirrincione, R. (2018). Comput. Geosci., 115, 56-65.
7. Shimizu I. (2008. Journal of Structural Geology, 30(7), 899-917.
8. Stöckhert B. & Duyster J. (1999). J. Struct. Geol. 21, 1477-1490.
9. Visalli R., (2018). Plinius, vol 44, DOI:10.19276/plinius.2018.01014
10. Wallis, S.R., 1995. Journal of Structural Geology 17, 1077e1093.